Analysis of the low-temperature specific heat of multiwalled carbon nanotubes and carbon nanotube ropes

Ari Mizel

Department of Physics, University of California at Berkeley, and Materials Sciences Division, Lawrence Berkeley National Laboratory, Berkeley, California 94720

Lorin X. Benedict

Department of Physics, University of California at Berkeley, and Materials Sciences Division, Lawrence Berkeley National Laboratory, Berkeley, California 94720
and Optical Technology Division, Physics Laboratory, National Institute of Standards and Technology, Gaithersburg, Maryland 20899

Marvin L. Cohen, Steven G. Louie, and A. Zettl

Department of Physics, University of California at Berkeley, and Materials Sciences Division, Lawrence Berkeley National Laboratory, Berkeley, California 94720

Nasser K. Budraa and W. P. Beyermann

Department of Physics, University of California at Riverside, Riverside, California 92521
(Received 14 December 1998)

We analyze specific-heat measurements in the temperature range $1 < T < 200$ K for two types of carbon nanotube samples: multiwalled tubes and ropes of single-walled tubes. The multiwalled tube sample has a specific-heat not unlike that of graphite, which we maintain is reasonable given the structural similarities between the two materials. In contrast, the low-temperature specific-heat data for ropes are surprisingly large in magnitude and have surprisingly strong temperature dependence. We present model calculations that highlight the puzzling nature of these results and then suggest explanations. [S0163-1829(99)00129-0]

I. INTRODUCTION

There is presently a great deal of interest in the physical properties of carbon nanotubes. Much of this interest derives from the development of a means of growing ropes of single-walled tubes with nearly uniform diameters.[1] These ropes are two-dimensional 2D hexagonal lattices of parallel carbon nanotubes with diameters ≈ 13.8 Å. They are grown with a laser vaporization technique. In contrast, the earliest production of carbon nanotubes[2] with an arc-discharge method yielded concentric multiwalled tubes with wide variations in size (diameters ranging from 40–300 Å). In researching carbon nanotubes, it is important to explore and to understand differences in the physical properties of the two sample types. For instance, the small diameters of tubes in the ropes may lead to electronic and vibrational densities of states markedly different from those of the larger multiwalled tubes. Also, the coupling between adjacent tubes in ropes should be quite different from the coupling between concentric tubes in a multiwalled sample.

In this work, we investigate these issues by studying the low-temperature specific heat of both sample types. The T dependence of $C(T)$ provides us with information about the low-energy excited states. There are two major kinds of excitations in these systems: electronic excitations and phonon excitations. Measurements of $C(T)$ yield insight into the densities of states associated with both kinds of excitations.

Experimentally, we find that $C(T)$ of multiwalled tubes is similar to that of graphite. We argue that indicates the low-energy electronic and phonon densities of states are probably little changed when flat graphene sheets are rolled into cylinders with diameters in the 40–300 Å range. In contrast, the measured $C(T)$ for the rope sample is larger than that of graphite and of multiwalled tubes for $T < 50$ K and has stronger temperature dependence. Above 50 K, the two samples are virtually indistinguishable. To analyze the behavior of the ropes, we develop a model calculation with no fitting parameters. The calculation shows that the rope $C(T)$ data are substantially larger than expected, and we indicate possible explanations.

II. EXPERIMENT

In this section, we present the measurements of $C(T)$ for multi-walled tube and rope samples. Sample preparation and characterization is outlined, followed by a discussion of the experimental technique. Results are then presented.

A. Sample preparation and characterization

1. Multiwalled carbon nanotubes

Multiwalled carbon nanotubes were synthesized in an arc-discharge chamber under 600 Torr helium pressure. A 1.25-cm diameter graphite electrode was arced against a water-cooled copper cathode, using 100-A dc current. With a gap between electrodes of about 1–2 mm, the electrode differential voltage was 18 V. Nanotube-rich material from the resulting boule was heated in air at 600 °C for 30 min to burn off undesirable nontube components. The nanotube samples were characterized by high-resolution transmission electron

microscopy; tubes were typically multiwalled with outer diameters of order 10–20 nm and lengths exceeding 10 μm.

2. Carbon nanotube ropes

Single-walled carbon nanotubes were synthesized using two different methods. In the arc-synthesis method, the procedure was similar to that used in multiwall carbon nanotube production; the most important difference was that the graphite anode was first drilled out and loaded with catalyst (either Co/Ni or Y/Ni). A sample of single-walled nanotubes, obtained from Rice University, was produced using a dual Nd/YAG laser vaporization technique.[1] The tube-rich material was purified by heating in vacuum for 30 min at 1000 °C. High-resolution transmission electron microscopy performed on the tubes revealed the well-known bundles or ''ropes'' of closely packed nanotubes with each rope containing on the order of 100 parallel tubes, each tube approximately 1.3 nm in diameter.

B. Experimental technique

A thermal relaxation technique was used to measure the specific heat from 0.6 to 210 K.[3] For each sample, ~1 kbar of pressure was used to press 10–20 mg of powder into a small cylindrical pellet with a diameter of ~3.2 mm. The pellet was attached to the sapphire platform of the calorimeter with a small amount of Apiezon[4] grease. In order to cover the whole temperature range, two calorimeters with different Cernox thermometers were used. The final data include corrections for τ_2 effects,[3] which arise because internal thermal impedances in the sample/platform system influence the approach to thermal equilibrium. Such effects are exacerbated by the porosity of the sample.

C. Results

In Fig. 1, $C(T)$ is plotted as a function of T for the different nanotube samples. On the same graph, a calculated specific heat for graphite is included[5] for comparison purposes. The three curves are similar, although the rope sample shows a larger $C(T)$ at small temperatures. When the data are plotted as $C(T)/T$ versus T in Fig. 2, it is evident that the specific heat at low temperatures for the rope sample is larger than that for the multiwalled nanotubes and graphite. In addition, the rope sample shows an interesting shoulder near 5 K. In Fig. 3, where $C(T)/T^2$ is plotted against T, the rope sample exhibits much stronger temperature dependence than the other two materials. The rope data show a pronounced peak around 2 K. Above approximately 50 K, in all three figures, the three samples appear essentially the same.

III. MODEL

In this section, we analyze the essential features of the results presented above. We first review some basic facts about the relationship between the specific heat and the density of states. Then, we comment on the similarity between graphite and the multiwalled tube sample. A model of the low-temperature phonon contribution to $C(T)$ for ropes is developed.
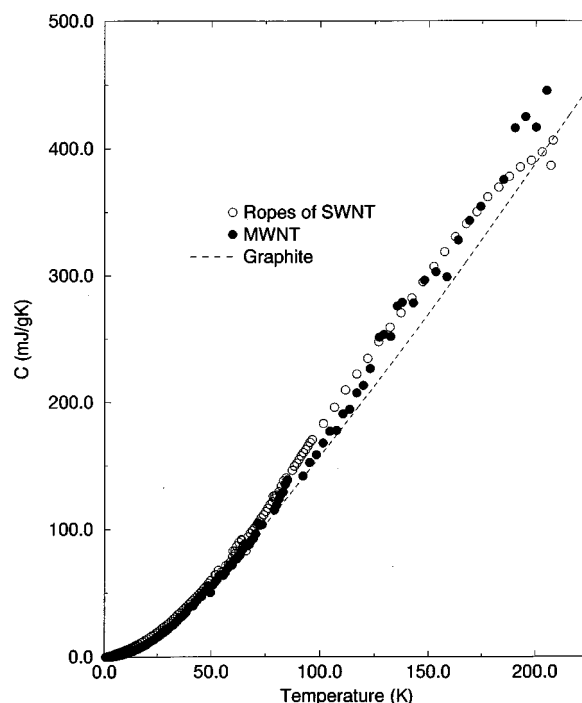

FIG. 1. Measured $C(T)$ versus T for ropes of single-walled nanotubes (SWNT) and for multiwalled nanotubes (MWNT). Lines connecting data points are a guide to the eye. Calculated graphite $C(T)$ from Nicklow, Wakabayashi, and Smith is included for comparison.

A. Specific heat and density of states

For a metallic system, the density of electronic states is nonzero at the Fermi energy, and this gives an electronic contribution to the specific heat that is linear in temperature.
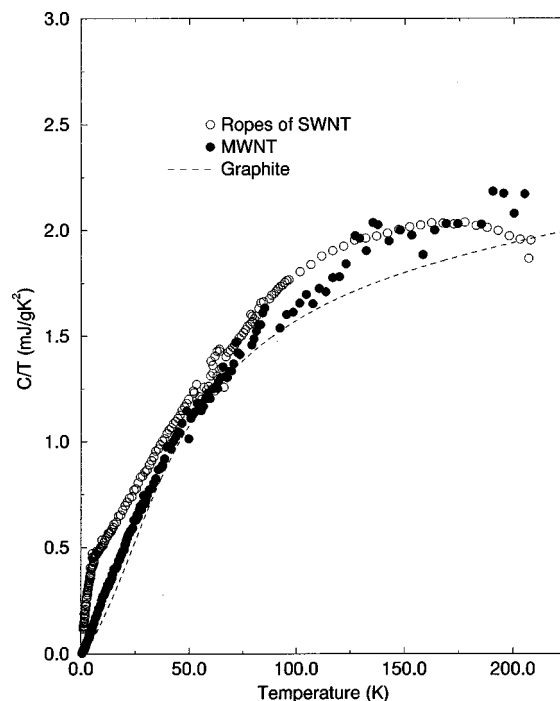

FIG. 2. Experimental $C(T)/T$ versus T for ropes of SWNT and for MWNT. Graphite calculation included.
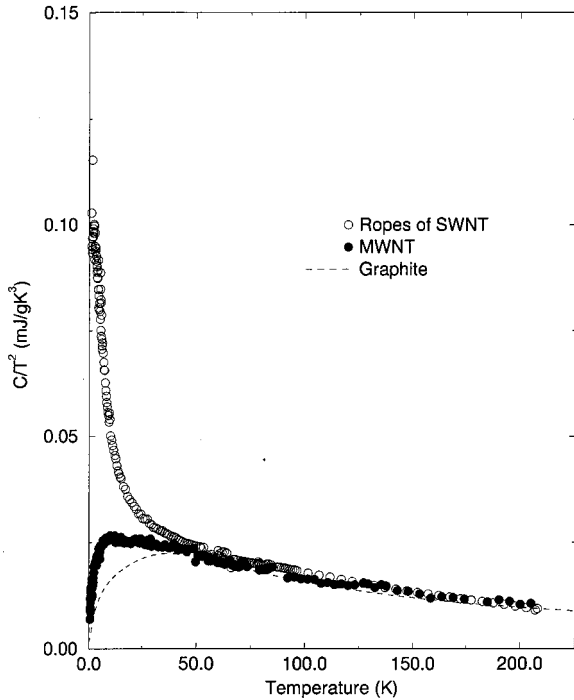
FIG. 3. Experimental $C(T)/T^2$ versus T for ropes of SWNT and for MWNT. Graphite calculation included.

Even for good metals, however, this behavior is only observable below a few Kelvin because phonon excitations dominate at higher temperatures. In this paper, we are concerned with graphitelike samples. Graphite is a semimetal with a small density of electronic states at the Fermi energy and has $C(T) \sim T$ below $T \sim 1.5$ K.[6] Thus the phonon contribution to the specific heat dominates even at relatively low temperatures. For this reason, we will focus on the vibrational specific heat in attempting to understand our data.

In the case of phonons, $C(T)$ typically follows T raised to some power higher than unity. The precise power depends on the detailed phonon dispersion relations and the dimensionality of the system. As is evident from our plots of the experimentally measured $C(T)/T$ and $C(T)/T^2$ versus T, complex behavior is seen in both multiwalled tube and rope samples for $T < 20$ K. To explain this behavior, it is necessary to study the low-energy vibrational modes of these samples; once the phonon density of states (PDOS) associated with these modes is determined, the vibrational specific heat is evaluated as follows.

The specific heat is defined as the temperature derivative of the energy density u:

$$C(T) = \frac{\partial u}{\partial T} = \frac{\partial}{\partial T} \int d\omega D(\omega) \frac{\hbar\omega}{\exp(\hbar\omega/kT) - 1}$$

$$= k \int d\omega D(\omega) \left[\frac{\left(\frac{\hbar\omega}{kT}\right)^2 \exp\left(\frac{\hbar\omega}{kT}\right)}{\left(\exp\left(\frac{\hbar\omega}{kT}\right) - 1\right)^2} \right], \quad (1)$$

where $D(\omega)$ is the phonon density of states. The factor in brackets is convolved with the density of states to obtain the specific heat. This ''heat-capacity convolution factor'' is ap-

preciable (> 0.1) for $\hbar\omega < 6kT$. For $\hbar\omega > 6kT$, the factor dampens out the contribution of $D(\omega)$ to the specific-heat integral. In this paper, we will be mainly concerned with features in $C(T)$ below 20 K, so we will consider the PDOS below 6×20 K ~ 10 meV. This is the energy range of long-wavelength acoustic phonons. Features in the excitation spectrum above this energy, like those arising from high-energy optical modes, will have little or no impact on the temperature region of interest. We will neglect them.

From the form of Eq. (1), it follows that, at low temperatures, $C(T)$ is proportional to T^{p+1} when $D(\omega)$ is proportional to ω^p. Thus, by plotting $C(T)$ divided by various powers of T, we gain insight into the frequency dependence of the PDOS.

B. Graphite and multiwalled tubes

The specific heat of graphite has been well characterized. One of the major contributions to this is the work of Nicklow, Wakabayashi, and Smith.[5] These authors use inelastic neutron-scattering data to fit force constants in a Born-von Karman force-constant model. From this, they calculate the PDOS and the resulting phonon contribution to the specific heat, $C^{ph}(T)$, where the ph superscript refers to phonons. We have used the force-constant model of Ref. 5 to calculate $C^{ph}(T)$ for graphite in the temperature range $1 < T < 200$ K. The results are plotted in Figs. 1–3 along with our nanotube data. The main feature in $C^{ph}(T)/T^2$ is the maximum at ~ 40 K. This results from a transition in the PDOS from $\omega^2 \rightarrow \omega^0$ behavior at $\hbar\omega = 16.3$ meV.

Figure 3 shows that both graphite and multiwalled carbon nanotubes exhibit a broad peak in $C(T)/T^2$ below 50 K. Although the peak associated with the multiwalled nanotube sample is somewhat sharper and at slightly lower temperature, the two curves are generally quite similar. The fact that $C(T)/T^2$ for multiwalled tubes can be compared favorably to $C^{ph}(T)/T^2$ for graphite implies two things. First, the electronic contribution to the multiwalled tube specific heat, $C^e(T)$, is small at these temperatures. This is to be expected, as remarked in the beginning of Sec. III A. It is supported experimentally by the nearly zero intercept of $C(T)/T$ versus T in the multiwalled nanotube curve of Fig. 2. Second, the similarity between $C(T)/T^2$ for multiwalled tubes and $C^{ph}(T)/T^2$ for graphite indicates that the PDOS of the two materials are similar. This is also not surprising, since the average radius of a tube in the sample is so large (~ 100 Å). Deviations from the flat graphene sheet PDOS have been predicted for isolated small radius single-walled carbon nanotubes,[7,8] but such sharp radius-dependent features should be averaged out in a sample with wide variations in tube radii. In short, $C(T)$ for the multiwalled tube sample looks much like $C^{ph}(T)$ for graphite, and this is to be expected.

C. Carbon nanotube ropes

In this section, we model the PDOS of ropes of single-walled nanotubes. Since the tubes in ropes have roughly the same diameter, 13.8 Å,[1] we first consider a single isolated tube of this size. Then, intertube forces are taken into account.
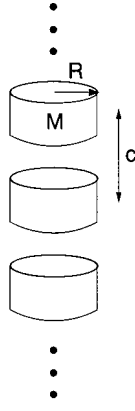
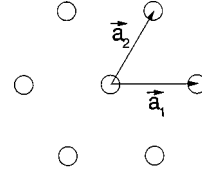FIG. 4. Coarse-grained model of a carbon nanotube.

FIG. 5. Cross-section of 2D hexagonal array of carbon nanotubes. Seven tubes are pictured to illustrate lattice structure. An actual rope includes on the order of 100 tubes.

1. Isolated carbon nanotube

An ideal, infinitely long nanotube has the following four phonon modes with $\omega(\mathbf{q}) \to 0$ as $\mathbf{q} \to 0$: A longitudinal acoustic (LA) mode, in which the tube is stretched and compressed along its axis; two transverse acoustic (TA) modes, in which the tube vibrates like a plucked string (the tube can be ''plucked'' in any direction perpendicular to its axis, so this mode is doubly degenerate); and a twist mode, in which portions of the tube are rotated by varying amounts about the tube axis. At exactly $\mathbf{q} = 0$, the LA mode is a rigid translation along the tube axis, the TA modes are translations perpendicular to the axis, and the twist mode is a rigid rotation about the axis. In order to understand the low-temperature specific heat of a rope sample, we do not need to consider the numerous optical modes that do not have $\omega(\mathbf{q}) \to 0$ as $\mathbf{q} \to 0$ (see Sec. III A). Indeed, the calculations of Ref. 8 show that the lowest energy for optical modes of tubes of this size is greater than 10 meV, which must be inactive for low temperatures.

Because the LA and twist modes involve atoms moving along the cylindrical surface of the undistorted tube, these modes can be approximately derived by folding the graphite in-plane LA and TA modes, respectively.[9] The neutron-scattering measurements of Nicklow, Wakabayashi, and Smith[5] provide an estimate of the sound velocities of these modes, v_{LA} (graphite) $\approx 2.5 \times 10^6$ cm/s, and v_{TA} (graphite) $\approx 1.5 \times 10^6$ cm/s. We would expect these velocities to be similar to v_{LA} (tube) and v_{twist} (tube). The tube LA mode sound velocity has been calculated for tubes in the size range of interest with a reliable tight-binding molecular-dynamics scheme.[7] The result for 13–14 Å diameter tubes is v_{LA} (tube) $\approx 1.7 \times 10^6$ cm/s, which is smaller than, but comparable to, the neutron-scattering result for v_{LA} (graphite). In addition, Ref. 7 finds the tube TA mode sound velocity to be v_{TA} (tube) $\approx 7.5 \times 10^5$ cm/s. The sound velocities computed by Saito et al.[8] are in reasonable agreement with these values. For our simple force-constant model, we shall take the three tube sound velocities to be v_{LA} (tube) $= 2 \times 10^6$ cm/s, v_{twist} (tube) $= 1 \times 10^6$ cm/s, and v_{TA} (tube) $= 8 \times 10^5$ cm/s.

To introduce the simplest picture that will include four acoustic branches, we model a tube as a 1D array of rings of radius R, and mass M, spaced a length c apart (see Fig. 4). Each ring is intended to represent a full unit cell of the nano-

tube; by neglecting the internal structure of the rings, we avoid the distraction of the tube's high-energy optical modes. The ring parameters are chosen to take the values $R = 7$ Å, $M = 40 m_c = 8 \times 10^{-22}$ g, and $c = 2.5$ Å, based upon the properties of a $(10,10)$ nanotube. Each ring has four degrees of freedom, expressed as coordinates (x, y, z, θ). The first three are the Cartesian positions of the center of mass of the ring, and θ is the angle of rotation about the tube axis ($\hat{\mathbf{z}}$). We define these coordinates to be displacements away from equilibrium. The Hamiltonian takes the form

$$H = \sum_l \frac{1}{2M} \mathbf{p}_{l\mathbf{c}}^2 + \frac{1}{2MR^2} L_{l\mathbf{c}}^{z\,2} + \frac{1}{2} M \frac{v_{TA}^2}{c^2} (x_{(l+1)\mathbf{c}} - x_{l\mathbf{c}})^2$$

$$+ \frac{1}{2} M \frac{v_{TA}^2}{c^2} (y_{(l+1)\mathbf{c}} - y_{l\mathbf{c}})^2 + \frac{1}{2} M \frac{v_{LA}^2}{c^2} (z_{(l+1)\mathbf{c}} - z_{l\mathbf{c}})^2$$

$$+ \frac{1}{2} MR^2 \frac{v_{twist}^2}{c^2} (\theta_{(l+1)\mathbf{c}} - \theta_{l\mathbf{c}})^2. \qquad (2)$$

Here, l is an integer, and $\mathbf{c} \equiv c\hat{z}$ is a vector pointing from one ring to the next, so that $l\mathbf{c}$ indexes a particular ring in the tube. L^z refers to the angular momentum of a ring about the z axis. This Hamiltonian yields four acoustic phonon branches, with sound speeds v_{LA}, v_{TA}, v_{TA}, and v_{twist}.

2. Hexagonal array of carbon nanotubes

A carbon nanotube rope is a collection of roughly 100 to 500 parallel tubes arranged in a 2D hexagonal array and separated by a center-to-center distance of $a = 17$ Å.[1] Here, we will neglect the rope surface and approximate the rope by an infinite lattice (see Fig. 5). The neglect of the surface introduces little error into the PDOS.[10] Each tube in the rope is modeled by the linear chain of rings described above. The equilibrium location of each ring in a rope is specified by a vector $\mathbf{r} = j\mathbf{a}_1 + k\mathbf{a}_2 + l\mathbf{c}$, where $\mathbf{a}_1 \equiv a\hat{x}$, $\mathbf{a}_2 \equiv a[(1/2)\hat{x} + (\sqrt{3}/2)\hat{y}]$, and j, k, and l are integers. The integers j and k identify a tube in the rope, and the integer l identifies a ring within a given tube.

There are two additional kinds of potential energy terms that must be added to the Hamiltonian (2) to account for intertube coupling. The first is a compression term, which enforces the tendency for tubes to be a distance a apart. The second is a shearing term, which imposes an energetic cost when tube surfaces are sheared past each other. The Hamiltonian becomes

$$H = \sum_{\mathbf{r}=j\mathbf{a}_1+k\mathbf{a}_2+l\mathbf{c}} \frac{1}{2M}\mathbf{p}_{\mathbf{r}}^2 + \frac{1}{2MR^2}L_{\mathbf{r}}^{z2} + \frac{1}{2}M\frac{v_{TA}^2}{c^2}(x_{\mathbf{r}+\mathbf{c}}-x_{\mathbf{r}})^2 + \frac{1}{2}M\frac{v_{TA}^2}{c^2}(y_{\mathbf{r}+\mathbf{c}}-y_{\mathbf{r}})^2 + \frac{1}{2}M\frac{v_{LA}^2}{c^2}(z_{\mathbf{r}+\mathbf{c}}-z_{\mathbf{r}})^2$$

$$+ \frac{1}{2}MR^2\frac{v_{twist}^2}{c^2}(\theta_{\mathbf{r}+\mathbf{c}}-\theta_{\mathbf{r}})^2 + \frac{1}{2}\kappa_{comp}(x_{\mathbf{r}+\mathbf{a}_1}-x_{\mathbf{r}})^2 + \frac{1}{2}\kappa_{comp}(x_{\mathbf{r}+\mathbf{a}_2}-x_{\mathbf{r}})^2 + \frac{1}{2}\kappa_{comp}(x_{\mathbf{r}+\mathbf{a}_2-\mathbf{a}_1}-x_{\mathbf{r}})^2$$

$$+ \frac{1}{2}\kappa_{comp}(y_{\mathbf{r}+\mathbf{a}_1}-y_{\mathbf{r}})^2 + \frac{1}{2}\kappa_{comp}(y_{\mathbf{r}+\mathbf{a}_2}-y_{\mathbf{r}})^2 + \frac{1}{2}\kappa_{comp}(y_{\mathbf{r}+\mathbf{a}_2-\mathbf{a}_1}-y_{\mathbf{r}})^2 + \frac{1}{2}\kappa_{shear}(\mathbf{u}_{\mathbf{r}+\mathbf{a}_1,\mathbf{r}})^2 + \frac{1}{2}\kappa_{shear}(\mathbf{u}_{\mathbf{r}+\mathbf{a}_2,\mathbf{r}})^2$$

$$+ \frac{1}{2}\kappa_{shear}(\mathbf{u}_{\mathbf{r}+\mathbf{a}_2-\mathbf{a}_1,\mathbf{r}})^2. \tag{3}$$

In the last few terms, we introduce the vector $\mathbf{u}_{\mathbf{r}_1,\mathbf{r}_2}$, the shear displacement between neighboring points on rings $\mathbf{r}_1$ and $\mathbf{r}_2$ when the rings shift and rotate. Shear can result from a combination of translations and rotations, so $\mathbf{u}_{\mathbf{r}_1,\mathbf{r}_2}$ involves (x,y,z) coordinated as well as θ coordinates:

$$\mathbf{u}_{\mathbf{r}_1,\mathbf{r}_2} = \frac{R}{|\mathbf{r}_{12}|}\left(r_{12,y}(\theta_{\mathbf{r}_1}+\theta_{\mathbf{r}_2}) + \frac{2r_{12,y}^2}{|\mathbf{r}_{12}|^2}(x_{\mathbf{r}_1}-x_{\mathbf{r}_2})\right.$$
$$\left. - \frac{2r_{12,x}r_{12,y}}{|\mathbf{r}_{12}|^2}(y_{\mathbf{r}_1}-y_{\mathbf{r}_2})\right)\hat{x}$$
$$+ \frac{R}{|\mathbf{r}_{12}|}\left(-r_{12,x}(\theta_{\mathbf{r}_1}+\theta_{\mathbf{r}_2}) + \frac{2r_{12,x}^2}{|\mathbf{r}_{12}|^2}(y_{\mathbf{r}_1}-y_{\mathbf{r}_2})\right.$$
$$\left. - \frac{2r_{12,x}r_{12,y}}{|\mathbf{r}_{12}|^2}(x_{\mathbf{r}_1}-x_{\mathbf{r}_2})\right)\hat{y} + (z_{\mathbf{r}_1}-z_{\mathbf{r}_2})\hat{z}, \tag{4}$$

where we have abbreviated $\mathbf{r}_{12}=\mathbf{r}_1-\mathbf{r}_2$. Equation (3) provides a reasonable phenomenological representation of the low-energy phonons in a carbon nanotube rope. By including the important binding forces in a standard fashion as two-body energy terms and choosing parameters appropriately, a quantitative modeling of the specific heat should be possible as in Ref. 5. Two new force constants enter into Eq. (3), κ_{comp} and κ_{shear}. They are each chosen by fitting to analogous graphite modes measured by Nicklow, Wakabayashi, and Smith.[5] The compression mode is analogous to the c axis LA mode in graphite. For the c axis LA mode in graphite, the spring connecting a unit cell in one sheet to an adjacent sheet has a spring constant of 5.8×10^3 dyn/cm. Assuming that the same type of spring connects rings in two adjacent tubes, we approximate $\kappa_{comp}=6\times10^3$ dyn/cm. This choice is physically reasonable, and the resulting value of κ_{comp} agrees well with the calculations of Charlier, Gonze, and Michenaud for the energetics of a hexagonal lattice of 4.1 Å radius tubes.[11] The shearing mode force constant κ_{shear} is similarly chosen. This mode is analogous to the c axis TA mode in graphite. Referring to Nicklow, Wakabayashi, and Smith, we take $\kappa_{shear}=8\times10^2$ dyn/cm. These choices for κ_{comp} and κ_{shear} are physically reasonable, and our theoretical heat capacity does not depend sensitively upon them (see Fig. 7).

The calculated low-frequency phonon band structure is plotted in Fig. 6. Note that the bands disperse much more for $\mathbf{q}$ along the tube axis than for $\mathbf{q}$ perpendicular to the axis. This is because intratube forces are much stronger than intertube forces. Note also that there are three modes with $\omega(\mathbf{q}\rightarrow0)=0$, rather than the four modes of an isolated tube. The twist mode is no longer acoustic, because of the presence of a nonzero κ_{shear}. The three lowest modes for $\mathbf{q}$ perpendicular to the tube axis are all modes in which the tubes are rigidly displaced and are ''bumping into'' adjacent tubes. These low-frequency, nondispersive modes give rise to prominent structure in the low-energy PDOS.

3. $C^{ph}(T)$ for hexagonal array of carbon nanotubes

The calculated PDOS for the hexagonal array can be substituted into Eq. (1) to obtain $C^{ph}(T)$, the temperature-dependent phonon contribution to the specific heat. We plot
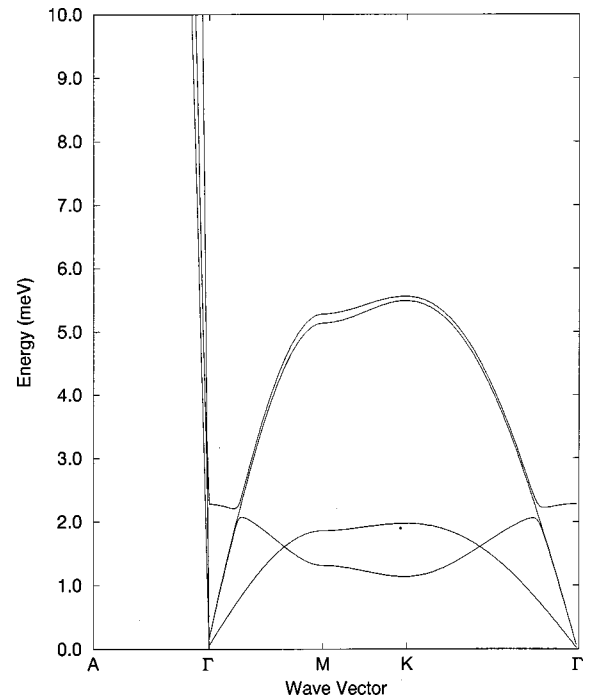

FIG. 6. Calculated low-frequency phonon band structure for infinite hexagonal lattice of carbon nanotubes with radii = 7 Å. Wave vectors along ΓA are parallel to the tube axis. All other wave vectors are perpendicular to the tube axis.
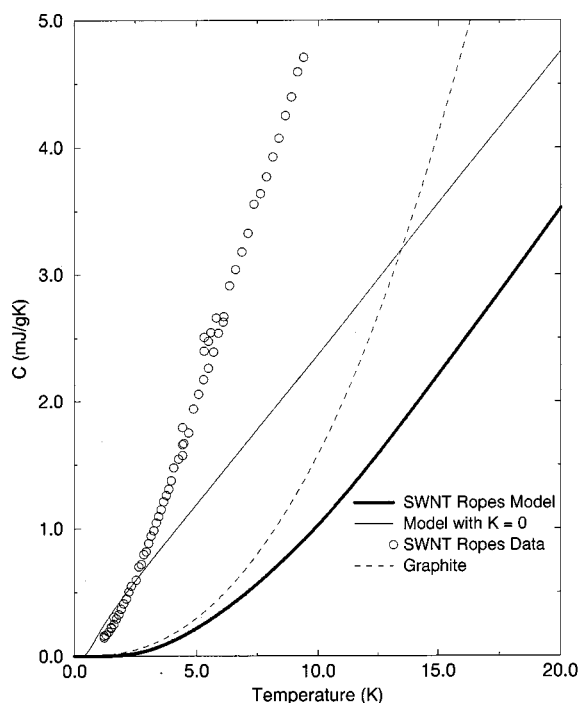
FIG. 7. Calculated $C(T)$ versus T for model of infinite hexagonal lattice of carbon nanotubes with radii = 7 Å compared to experimental data. $K=0$ curve gives results of model calculation with κ_{comp} and κ_{shear} reduced to nearly zero.

$C^{ph}(T)$ in Fig. 7, along with the experimental result. The low-temperature rope specific heat is predicted to be substantially lower than that of graphite, because tubes should lack the low-energy ''carpet-ripple'' modes that exist in a graphite sheet. This prediction does not agree with experiment; the experimental heat capacity for ropes substantially exceeds that for graphite.

To test the robustness of the model, we compute the specific heat with κ_{comp} and κ_{shear} both set infinitesimally small. It is important to assess the sensitivity of our results to these parameters in particular because they are difficult to estimate accurately. The increase in the specific heat that results from softening the intertube springs is shown in Fig. 7. Even this increase is insufficient to bring about agreement between theory and experiment.

Our experimental results are therefore somewhat puzzling. Since there has been some consideration of electron

correlation in nanotubes,[12] one might entertain the possibility that electronic effects are responsible for the disagreements between model and experiment. As remarked in the beginning of Sec. III A, one expects the electronic contribution to the specific heat of a graphitelike sample to be minor. This expectation appears to be borne out in the case of multiwalled tubes. It therefore seems unlikely that electronic effects are making appreciable contributions to our rope sample measurements, especially at relatively high temperatures like 20 K. However, the magnitude of such effects could be checked in the future by extending our specific-heat measurements to lower temperatures. Finally, we note that some of the sample may include material other than carbon nanotubes. The admixture of nontubelike material would change the density of excited states, and complicate the analysis. For example, molecules like methane possess specific heats which exceed that of graphite by more than a factor of 4 even at room temperature. If a large fraction of the rope sample were include such molecules, the sample would exhibit a markedly enhanced low-temperature heat capacity.

IV. CONCLUSION

We present measurements of the specific heat of two kinds of carbon nanotube samples. The data for multiwalled nanotubes are found to agree generally with the behavior of graphite. For ropes of single walled tubes, the specific heat is found to exceed that of graphite at low temperatures, and $C(T)/T^2$ is found to peak at a lower temperature than for graphite. A model calculation of the long-wavelength vibrations of a rope of carbon nanotubes highlights the surprising nature of the experimental results.

[1] A. Thess, R. Lee, P. Nikolaev, H. Dai, P. Petit, J. Robert, C. Xu, Y. H. Lee, S. G. Kim, A. G. Rinzler, D. T. Colbert, G. E. Scuseria, D. Tomzak, J. E. Fischer, and R. E. Smalley, Science **273**, 483 (1996).

[2] S. Iijima, Nature (London) **354**, 56 (1991).

[3] R. Bachman *et al.*, Rev. Sci. Instrum. **43**, 205 (1972).

[4] Certain commercial equipment, instruments, or materials are identified in this paper to foster understanding. Such identification does not imply recommendation or endorsement by the National Institute of Standards and Technology, nor does it imply that the materials or equipment identified is necessarily the best available for the purpose.

[5] R. Nicklow, N. Wakabayashi, and H. G. Smith, Phys. Rev. B **5**, 4951 (1972).

[6] W. DeSorbo and G. E. Nichols, J. Phys. Chem. Solids **6**, 352 (1958).

[7] J. Yu, R. K. Kalia, and P. Vashishta, J. Chem. Phys. **103**, 6697 (1995).

[8] R. Saito, T. Takeya, T. Kimura, G. Dresselhaus, and M. S. Dresselhaus, Phys. Rev. B **57**, 4145 (1998).

[9] This simply follows from applying a band-folding argument to the graphene sheet phonon modes, as discussed in L. X. Benedict, S. G. Louie, and M. L. Cohen, Solid State Commun. **100**, 177 (1996). However, this argument *cannot* be applied to the

tube TA mode, for it involves atoms moving perpendicular to the sheet plane. This point was not addressed in the above publication.

[10] We confirmed this physically reasonable assertion numerically.

[11] J.-C. Charlier, X. Gonze, and J.-P. Michenaud, Europhys. Lett. **29**, 43 (1995).

[12] Yu. A. Krotov, D.-H. Lee, and S. G. Louie, Phys. Rev. Lett. **78**, 4245 (1997); L. Balents and M. P. A. Fisher, Phys. Rev. B **55**, R11 973 (1997); R. Egger and A. O. Gogolin, Phys. Rev. Lett. **79**, 5082 (1997); C. Kane, L. Balents, and M. P. A. Fisher, *ibid.* **79**, 5086 (1997).